Research Article

SOHAG JOURNAL OF SCIENCES

https://doi.org/10.21608/sjsci.2024.337192.1235

Sacrificial Template Effect on the Synthesis of Nickel Oxide Nanoparticles as an Efficient Catalyst for Hydrogen Peroxide Decomposition

Hatem A. Mahmoud[1], Aya Adel A. Ali[1,*], Tarek T. Ali[1], Bahaa M. Abu-Zied[2]

[1] *Chemistry Department, Faculty of Science, Sohag University, Sohag 82524, Egypt*
[2] *Chemistry Department, Faculty of Science, Assiut University, 71516 Assiut, Egypt*
[*]*Email: aya2016091@science.sohag.edu.eg*

Received: 21st November 2024, **Revised:** 23rd December 2024, **Accepted:** 28th December 2024
Published online: 24th January 2025

Abstract: In this study, the impact of urea and 2-hydroxyethyl cellulose as precipitating and stabilizing agents on the morphology and catalytic efficiency of nickel oxide (NiO) nanoparticles was explored under hydrothermal conditions at 130 °C for 13 hours. The structural and morphological properties of the synthesized NiO were characterized using X-ray diffraction (XRD), Fourier transform infrared spectroscopy (FT-IR), and transmission electron microscopy (TEM), revealing distinct differences in particle size and shape. TEM analysis showed that NiO synthesized with urea (NU-C) exhibited a more uniform shape compared to that synthesized with 2-hydroxyethyl cellulose (NH-C). Catalytic activity was evaluated through the decomposition of hydrogen peroxide (H_2O_2) in the presence of dispersed NiO powders. Kinetic studies demonstrated that the reaction rate constant for NU-C was approximately 1.5 times higher than that for NH-C, highlighting the superior catalytic efficiency of the urea-based NiO. The activation energies and thermodynamic parameters (ΔH, ΔS, and ΔG) were determined via Arrhenius plots, indicating that the differences in activation energy correlated with the morphological variations. These findings suggest that the shape and size of NiO nanoparticles play a critical role in enhancing their catalytic performance in H_2O_2 decomposition.
Keywords: Nickel oxide, Urea, 2-hydroxyethyl cellulose, Hydrothermal method.

1. Introduction

Over the last decade, nanomaterials have been considered a promising study subject with multiple potential applications in different fields ranging from electronics and photonics to catalysis and medicine. Nanoscale of metals, metal oxides, and nanocomposites have proven to be more effective and efficient than their bigger counterparts [1]. According to the US National Science Foundation, nanomaterials show three important features: they must have at least one dimension between 1 and 100 nm; methodologies for design that provide fundamental control over both the chemical and physical characteristics of molecular structures; and the ability to combine and form larger structures [2]. The methods to synthesize NPs can include chemical, physical, and green processes. Physical synthesis involves a top-down approach, while chemical synthesis involves a bottom-up approach. As a result, scientists usually prefer the bottom-up approach, where NPs are formed atom-by-atom, molecule-by-molecule, or cluster-by-cluster, using methods such as chemical precipitation, sol-gel method, hydrothermal process, thermal decomposition, microwave-assisted synthesis, and spray pyrolysis. [3-5]

Nanosized crystalline metal oxides, in particular, have gained growing attention because of their enormous surface areas, distinct adsorptive features surface flaws, and rapid diffusivities [6]. In recent years, researchers have increasingly focused on transition metal oxides (TMOs) as nanomaterials, which exhibit diverse structures and properties and find applications in various industries such as engineering, electronic industry, chemical industry, medicine, energy, and catalysis [7-9]. Nickel oxide is an admired TMO because of its superior ferromagnetic characteristics, large coercive forces, and chemical stability [6, 8-16] . NiO NPs are used extensively in modern-day technology as inexpensive catalysts that drive reactions through alternate pathways, thanks to their natural abundance[17].

NiO NPs have also been shown to be effective in the degradation of various dyes, through photocatalytic processes[18, 19]. Furthermore, NiO NPs have been found to facilitate the decomposition of hydrogen peroxide (H_2O_2)[20], which is widely recognized as an environmentally benign reagent due to its degradation, which usually results in the production of water and oxygen. In industry, hydrogen peroxide finds primary application as an oxidizing agent, as well as a disinfectant and sterilant, either in its pure form or as peracids like peracetic acid. It is particularly favored as a reagent in wastewater treatment [21].To ensure safe disposal after industrial use, diluted hydrogen peroxide (H_2O_2) must be used in the decomposition process. Several catalysts have been identified as effective agents for this decomposition process such as platinum which is considered a highly selective catalyst for H_2O_2 decomposition with a rate constant of 7.1×10^{-2} s^{-1}. According to[22] , palladium is superior to platinum in the decomposition of hydrogen peroxide. Manganese dioxide (MnO_2) is also a strong catalyst for the decomposition of H_2O_2.

At various pH levels of 3 to 10, the observed rate constants on MnO_2 were $1.5x10^{-4}$ s^{-1} to 9.7×10^{-4} s^{-1}, respectively [23]. Furthermore, ferric ions and iron oxide have been shown to catalyze the decomposition of H_2O_2, with the largest recorded rate constant of $2.7x10^{-3}$ s^{-1} [24, 25]. Other catalysts for the decomposition of hydrogen peroxide include iron-cobalt oxide [26]some rare earth perovskites[27], copper (II) ions[28], and water-ceramic interfaces [29]. Notably, activated carbon also exhibits H_2O_2 decomposition activity, with rate constants ranging from $6x10^{-4}$ to $3x10^{-2}$ s^{-1}[30] . Therefore, we have focused on nickel oxide in our study as an alternate catalyst and non-precious material which has remarkable activity in accelerating hydrogen peroxide decomposition and facilitating its broad application. NiO NPs were synthesized via the hydrothermal method, followed by calcination, and then characterized using various techniques. Fourier transform infrared spectroscopy (FT-IR) and XRD were used to investigate the structural identification and presence of the nickel oxide functional group respectively. TEM was used to study the size and shape of the produced nickel oxide particles. We also studied the influence of the template on the shape and particle size of the produced catalyst. The reaction rate constants at different temperatures were calculated, also we determined the Arrhenius parameters and standard enthalpies of activation for the reactions through studying the temperature dependence of the rate constants.

2. Materials and methods

2.1. Materials

All the substances used for this study were of good analytical quality, and no further purification processes were performed. Hydrogen peroxide, Urea, 2-hydroxyethyl cellulose (HEC), nickel nitrate hexahydrate ($Ni\ (NO_3)_2.6H_2O$), and aqueous Tetramethylammonium hydroxide are purchased from sigma Aldrich. For all solutions, distilled water was used.

2.2. catalyst preparation

Nickel oxide was produced using a hydrothermal approach. Urea and HEC were used as templates. First, 100 milliliters of distilled water were used to prepare a 0.021 mole nickel nitrate solution (solution A). At 60 °C, two grams of urea were dissolved in 100 ml of distilled water (solution B), and two grams of HEC were dissolved in another 100 ml of distilled water (solution C) until the template was entirely dissolved. The two solutions of (A, B) and (A, C) were mixed separately in a 250-ml Teflon line, and the pH was adjusted to 9 using tetramethylammonium hydroxide to ensure that a suitable base medium was available for the precipitation of nickel hydroxide. After a 13-hour autoclave process at 130°C, the sample was carefully filtered, rinsed with distilled water and ethanol, and then dried overnight in a drying oven at 110°C. The samples were labeled as NU-D and NH-D, where U, H, and D represent urea, 2-hydroxyethyl cellulose, and drying samples, respectively, and they were calcined at 400 °C for 3h isothermal with a rate of 1 °C/min. Samples were labeled as NU-C and NH-C respectively.

2.3. Instruments for Characterization

The crystalline structures of the produced products were examined using a D8-Advance XRD system with monochromatic Cu-Kα radiation (λ = 1.5418 Å), operated at a scan rate of 0.05°/min within a 2θ range of 20° to 80°. The average crystallite size of the NiO nanoparticles was determined from the broadening of the XRD peak using the Scherrer equation, with further verification provided by transmission electron microscopy (JEOL, model JEM 100CX II). Fourier transform infrared (FT-IR) spectroscopy was performed using a Bruker Alpha FT-IR spectrometer in the 400–4000 cm^{-1} range, utilizing KBr to identify the chemical functional groups present.

2.4. Catalytic Studies

The catalytic process of hydrogen peroxide is one of the most reliable, effective, long-lasting, and non-destructive processes available. This process provides the selective generation of oxygen molecules with high purity and continuous supply if the catalyst has not been destroyed either physically or contaminated in any way [31-34]**.** Deren et al. described the use of a closed-glass system to investigate the catalytic activity of the synthesized catalyst in the decomposition of H_2O_2 [35]. The system consists of two burettes (50 mL and 100 mL) filled with distilled water and a 150 mL tightly closed round bottom flask immersed in a water bath and connected to a manometer. The temperature of the water bath was adjusted at the specified temperature (35, 40, 45, and 50 °C) before the reaction flask was placed inside. Then 50 mg of the nickel oxide catalyst and 20 ml of 30% H_2O_2 were rapidly added to the catalyst vessel and tied to the glass apparatus. To calculate the volume of hydrogen evolved, the amount of water displaced by hydrogen was measured over time and the rate constant was calculated from the slope of the plot of volume versus time, assuming a zero-order reaction. The thermodynamic parameters for the catalytic decomposition reaction of the hydrogen peroxide by the produced nickel oxide nanoparticles were calculated using the Arrhenius equation [36].

$$lnk = lnA - \frac{E_a}{RT} \quad (1)$$

Where $\boldsymbol{A}$ refers to the Arrhenius constant, $\boldsymbol{k}$ is the reaction rate constant, $\boldsymbol{R}$ is the universal gas constant (8.314 J/mol K), $\boldsymbol{T}$ is the temperature of the reaction, and $\boldsymbol{E_a}$ refers to the activation energy of the reaction in J/mol.

The standard reaction enthalpies were calculated using the Eyring equation

$$ln\left(\frac{kh}{k_B T}\right) = \frac{\Delta S^*}{R} + \frac{-\Delta H^*}{RT} \quad (2)$$

where $\boldsymbol{k}$ is the rate constant, $\boldsymbol{T}$ is the absolute temperature, ($\boldsymbol{H^*}$) is the standard enthalpy of activation, ($\boldsymbol{k_B}$) is the Boltzmann constant, ($\boldsymbol{h}$) is the Planck constant, and ($\boldsymbol{S^*}$) is the standard entropy of activation. Gibbs energy of activation ($\boldsymbol{\Delta G^*}$) can be calculated using equation. **3**:

$$\Delta G^* = \Delta H^* - T\,\Delta S^* \quad (3)$$

3. Results and Discussion:

3.1. Catalyst characterization

The crystallinity of the produced materials was determined

by XRD before and after calcination in the angle of 2θ range between 20° - 80°. The XRD diffractograms of the produced materials before calcination, shown in Figure.1(a) for NU-D and Figure.1(b) for NH-D, are well-matched to JCPDS card NO. 00-014-0117. The XRD pattern indicates the presence of (011), (100), (101), (102), (110), (111), (103), and (201) diffraction planes, showing that the produced material before calcination is Ni $(OH)_2$. To obtain NiO, we have calcinated Ni $(OH)_2$ at 400 °C which yielded NiO. The XRD pattern in Figure.2 indicates the existence of (111), (200), (220), (311), and (222) diffraction planes so the successful transfer of Ni $(OH)_2$ to NiO was verified by the matching of this NiO XRD data to JCPDS card NO. 01-073-1523 for NU-C Figure.1(a) and NH-C Figure.2(a), respectively. Additionally, the expanded peaks in Figure.1 show the nanometer-sized crystallites. The Debye-Scherrer equation was used to determine the crystal size as follows:

$$d = \frac{K\lambda}{B\cos\theta} \quad (4)$$

where d is the grain size, $K = 0.89$ is the Scherrer constant, θ is the peak's diffraction angle, and λ is the wavelength of the X-ray (Cu Ka,1.54056 A°) B attitudes for the full width at half-height of the peaks (in radians). Table **1** displays the crystal size of the NiO sample, which was determined by applying the Debye-Scherrer equation.

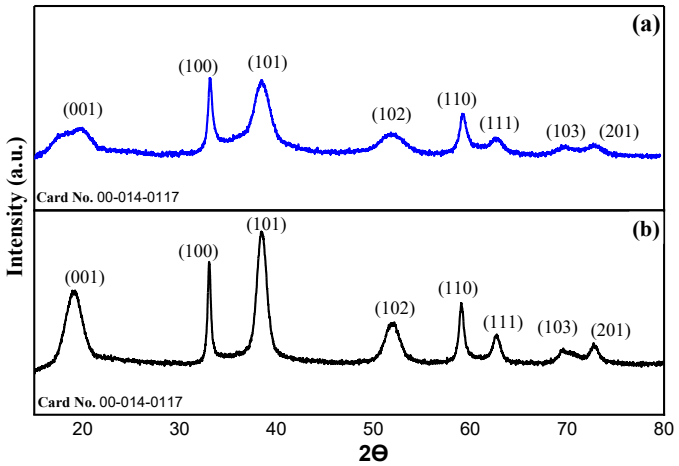

Fig.1. XRD patterns of (a) NU-D and (b) NH-D.

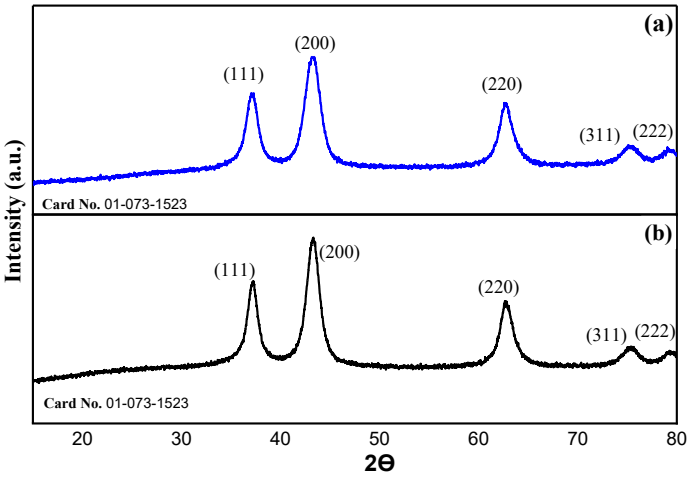

Fig.2. XRD patterns of (a) NU-C and (b) NH-C.

Table 1 Particle sizes of the synthesized materials

Catalyst	NU-D	NU-C	NH-D	NH-C
Particle size	26.33 nm	16.72 nm	16.46 nm	15.52 nm

The FT-IR spectra of the precursor Ni $(OH)_2$ and the oxide products NiO nanoparticles following calcination are shown in Figure.3, which was used to analyze the chemical bonding nature of the sample. The O–H stretching vibration of the H–bound OH group and the interlayer water molecules is attributed to the wide and powerful band with a center of around 3400 cm^{-1}. The bending of the interlayered H_2O molecules is responsible for the observed band that appeared at about 1630 cm^{-1} [37]. The C–O stretching vibration and the O–C=O symmetric and asymmetric stretching vibrations are attributed to the serrated absorption bands in the 1000–1500 cm^{-1} range [18]. It can be seen from Figure.3(b) and Figure.3(d) that the peaks at approximately 400 cm^{-1} and 800 cm^{-1} are assigned to the Ni–O stretching vibration also it is evident from the wide absorption band that the NiO particles are nanocrystals. The quantum size effect and spherical nanostructures of NiO nanoparticles cause their FT-IR absorption to be blue-shifted in comparison to the bulk form [18, 37]. The band about 1030 cm^{-1} and 1100 cm^{-1} are related to the stretching mode of Ni-O-Ni [38, 39]. While the band near 1630 cm^{-1} is associated with the H–O–H bending vibrations mode, which may be caused by water adsorption from the air or physical absorption of water by the calcined powders during the preparation of FT-IR sample disks, the broad and intense band around 3400 cm^{-1} is associated with the O–H stretching vibration of the interlayer water molecules [18, 40, 41].

TEM was used to analyze the produced nickel oxide's morphology and particle size. Figure.4 displays TEM images of NU-C and NH-C. The two catalysts obviously have different shapes. NU-C reveals that the surface is nanosheets without any voids, but NH-C reveals that the surface is nanorods.

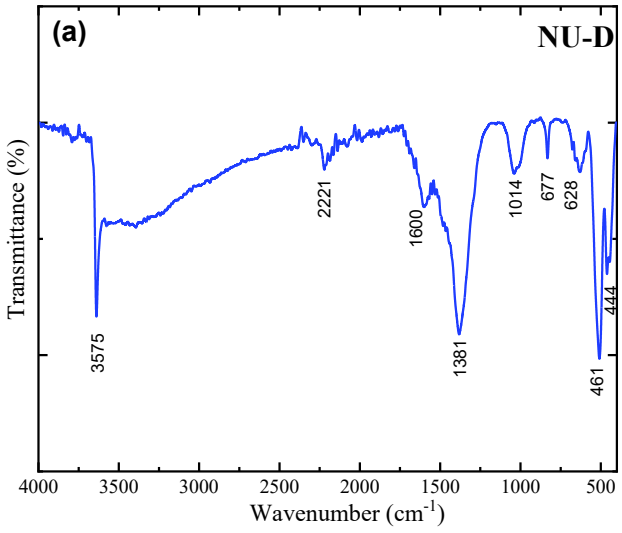

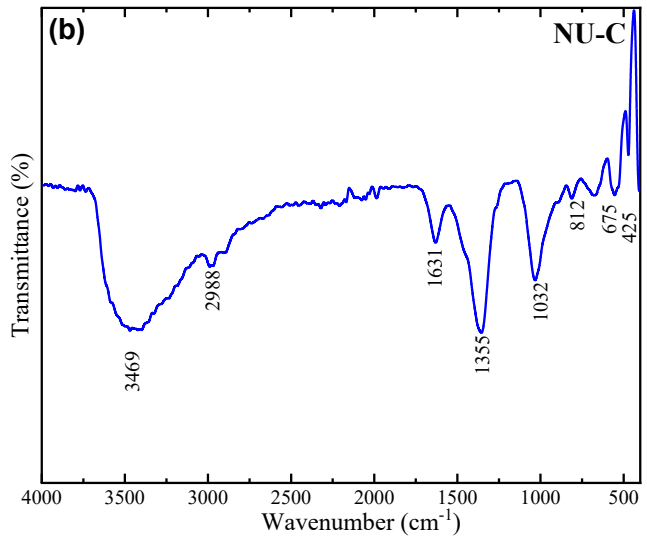

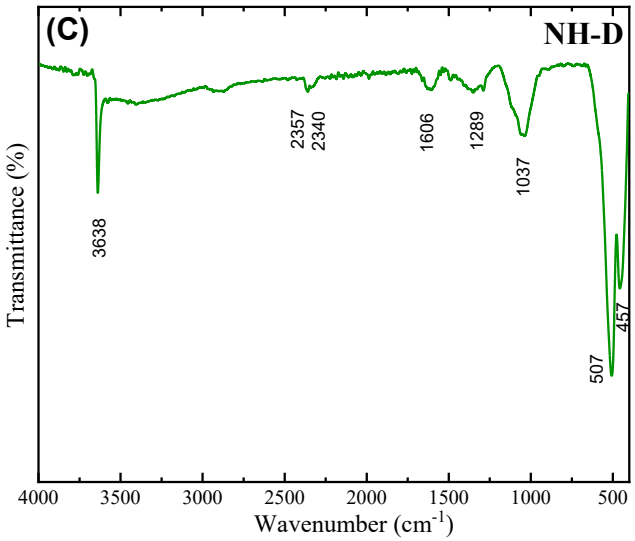

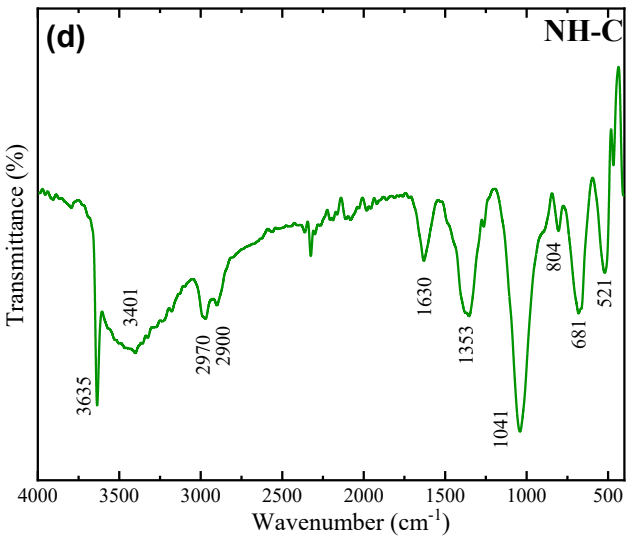

Fig.3 FT-IR spectra of (a) NU-D, (b) NU-C, (c) NH-D, and (d) NH-C

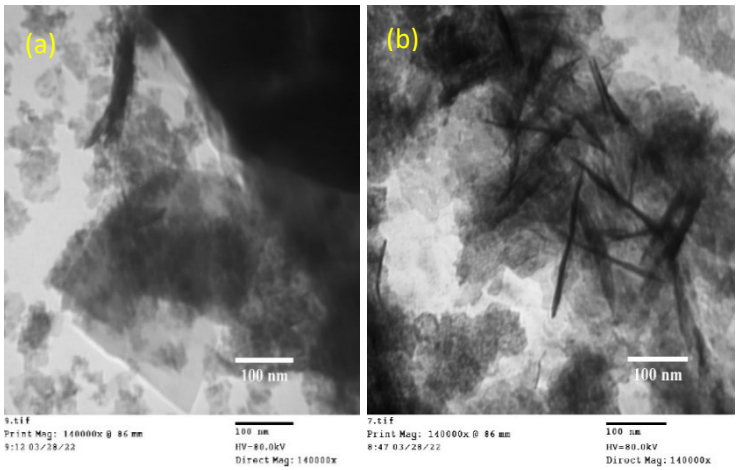

Fig. 4 TEM images of (a) NU-C, (b) NH-C catalyst.

3.2. Catalytic activity of the decomposition of hydrogen peroxide.

The time-dependent volume of oxygen evolution generated by the catalytic decomposition of hydrogen peroxide at various temperatures and ambient pressures. The Arrhenius activation energies were calculated graphically by plotting the logarithm of the zero-order rate constant as a function of inverse absolute temperature. The influence of temperature on the reaction rate constants of the two produced nickel oxides was studied at 308, 313, 318, and 323K.

The upper-temperature limit was defined as the lowest temperature at which sufficient data points could be collected to identify how the volume of oxygen changed over time, as the reaction develops too rapidly to enable appropriate data obtained above a specific temperature The Arrhenius plots are displayed in Figure.5(a),(b) and Table 2 displays the data that was obtained. The Eyring equation was used to calculate the standard reaction enthalpies of activation Figure.6(a),(b). For the two produced nickel oxides, the obtained Ea values differ considerably. The activation energy may probably be determined by the microstructural features of the particles, including the kind of atoms present at the catalytically active surface sites and the degree of hydroxylation at these sites [37]

Dissociative adsorption of H_2O results in hydroxylation, which is a process seen on the majority of metal oxide surfaces in aqueous solution [42]. The structure and extent of this hydroxylation layer determine the rigidity of the interfacial water layers, which are somewhat further away from the surface but still interact with the surface HO groups. The barrier for H_2O_2 diffusion through the adsorbed water interfacial layers before it reaches the catalytically active surface sites increases with the rigidity of the layers. As a result, it is estimated that the surface's attraction to water will influence the activation energy barriers for H_2O_2 decomposition. In addition, the intermediate products produced during the decomposition of H_2O_2 include oxygen species that, although being radicals, exhibit "water-like" characteristics, such as the capacity to form hydrogen bonds [43]. As mentioned before, the HO radical interacts with

the surface by creating bound states with exposed metal cations via an unpaired electron localized at the O atom. Even though H_2O is a molecular species, it has non-bonding electrons that are more localized at its O atom, and the more exothermic type of interaction between an H_2O molecule and the surface occurs because of the interaction of these electrons with the available orbitals of exposed surface metal atoms.

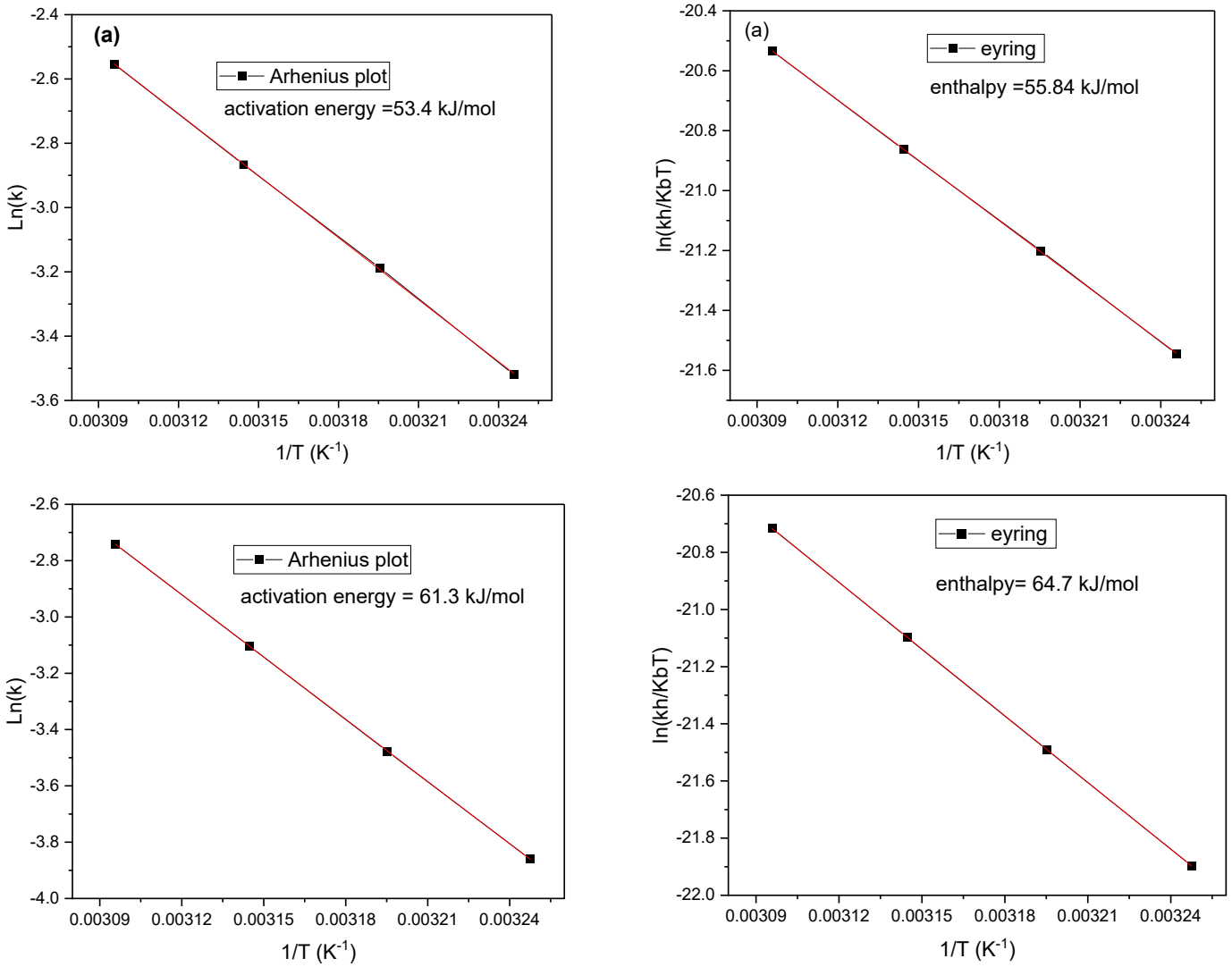

Fig.5 Arrhenius plot for (a) NU-C, and (b) NH-C catalyst.

Fig.6 Eyring plot for (a) NU-C, and (b) NH-C catalyst.

Table 2: Thermodynamic parameters for the decomposition of H_2O_2 catalyzed by the synthesized catalysts

Synthesized catalyst	T (K)	Rate constant	Ea (kJ/mol)	A (s^{-1})	ΔH^* (kJ/mol)	ΔS^* (kJ/mol)	ΔG^* (kJ/mol.K)
NU-C	308	0.028	53.4	$3.21*10^7$	55.84	0.0022	55.17
	313	0.039					55.16
	318	0.052					55.15
	323	0.084					55.14
NH-C	308	0.021	61.3	$5.30*10^8$	64.72	0.0281	56.07
	313	0.026					55.94
	318	0.036					55.79
	323	0.068					55.65

4. Conclusion

Nickel oxide was produced through the hydrothermal technique at temperatures of 130 °C for 13 hours using urea and 2-hydroxy ethyl cellulose as templates. Subsequently, the samples were calcined at 400 °C with a rate of 1 °C/min and held isothermally for three hours. These samples were labeled as NU-C and NH-C. The synthesized nickel oxide displayed moderate activity in the decomposition of hydrogen peroxide, with activity being influenced by the template used in the preparation method. Thermal analysis of the hydrolysis process revealed that all three samples exhibited a low activation energy below 62 kJ mol^{-1}.

CRediT authorship contribution statement:

Conceptualization, Tarek T. Ali and Aya Adel A. Ali.; methodology, Aya Adel A. Ali.; software, Hatem A. Mahmoud.; validation, Tarek T. Ali., Bahaa M. Abu-Zied. and Aya Adel A. Ali.; formal analysis, Hatem A. Mahmoud.; investigation, Aya Adel A. Ali.; resources, Bahaa M. Abu-Zied., Hatem A. Mahmoud; data curation, Aya Adel A. Ali.; writing—original draft preparation, Tarek T. Ali., Aya Adel A. Ali; writing—review and editing, Bahaa M. Abu-Zied., Tarek T. Ali., Hatem A. Mahmoud.; visualization, Bahaa M. Abu-Zied., Hatem A. Mahmoud.; supervision, Tarek T. Ali., Hatem A. Mahmoud., Bahaa M. Abu-Zied.. All authors have read and agreed to the published version of the manuscript."

Data availability statement

The data used to support the findings of this study are available from the corresponding author upon request.

Declaration of competing interest

The authors declare that they have no known competing financial interests or personal relationships that could have appeared to influence the work reported in this paper.

Acknowledgments

The authors extend profound gratitude to Sohag University for its essential support of the current study.

References

[1] W. Ahmad, K. Kumar Jaiswal, M. Amjad, I*norganic and Nano-Metal Chemistry*, 51 (2021) 1147-1154.
[2] H. Alinezhad, K. Pakzad, M. Nasrollahzadeh, *Applied Organometallic Chemistry*, 34 (2020) e5473.
[3] I. Ijaz, E. Gilani, A. Nazir, A. Bukhari, *Green chemistry letters and reviews*, 13 (2020) 223-245.
[4] J. Wilcoxon, *Frontiers of nanoscience*, Elsevier2012, pp. 43-127.
[5] S. Bhatia, S. Bhatia, *Natural polymer drug delivery systems: Nanoparticles, plants, and algae*, (2016) 33-93.
[6] Y. Wu, Y. He, T. Wu, T. Chen, W. Weng, H. Wan, *Materials Letters*, 61 (2007) 3174-3178.
[7] M. Nasrollahzadeh, M. Sajjadi, S. Iravani, R.S. Varma, *Journal of hazardous materials*, 401 (2021) 123401.
[8] Q. Li, L.-S. Wang, B.-Y. Hu, C. Yang, L. Zhou, L. Zhang, *Materials Letters*, 61 (2007) 1615-1618.
[9] X. Xin, Z. Lü, B. Zhou, X. Huang, R. Zhu, X. Sha, Y. Zhang, W. Su, *Journal of Alloys and Compound*s, 427 (2007) 251-255.
[10] X. Ni, Y. Zhang, D. Tian, H. Zheng, X. Wang, *Journal of Crystal Growth*, 306 (2007) 418-421.
[11] S. Thota, J. Kumar, J*ournal of physics and chemistry of solids*, 68 (2007) 1951-1964.
[12] S.A. Needham, G. Wang, H.-K. Liu, *Journal of Power Sources*, 159 (2006) 254-257.
[13] Y.-Z. Zheng, M.-L. Zhang, *Materials Letters*, 61 (2007) 3967-3969.
[14] I. Hotovy, J. Huran, L. Spiess, H. Romanus, D. Buc, R. Kosiba, *Thin Solid Films*, 515 (2006) 658-661.
[15] K.-C. Min, M. Kim, Y.-H. You, S. Lee, Y. Lee, T.-M. Chung, C. Kim, J.-H. Hwang, K.-S. An, N.-S. Lee, S*urface and Coatings Technology*, 201 (2007) 9252-9255.
[16] E. Souza, J. Duque, L. Kubota, C. Meneses, *Journal of physics and chemistry of solids*, 68 (2007) 594-599.
[17] A. Haider, M. Ijaz, S. Ali, J. Haider, M. Imran, H. Majeed, I. Shahzadi, M.M. Ali, J.A. Khan, M. Ikram, *Nanoscale research letters*, 15 (2020) 1-11.
[18] S.D. Khairnar, V.S. Shrivastava, *Journal of Taibah University for Science*, 13 (2019) 1108-1118.
[19] N.A. Khan, K. Saeed, I. Khan, T. Gul, M. Sadiq, A. Uddin, I. Zekker, *Applied Water Science*, 12 (2022) 131.
[20] K. AKHTER, *Journal of the Chemical Society of Pakistan*, 31 (2011) 59.
[21] M. Rigoletto, E. Laurenti, M.L. Tummino, *Catalysts*, 14 (2024) 267.
[22] A. Plauck, E.E. Stangland, J.A. Dumesic, M. Mavrikakis, *Proceedings of the National Academy of Sciences*, 113 (2016) E1973-E1982.
[23] M. ALI, N. Khalid, K. AKHTAR, *Journal of The Chemical Society of Pakistan*, 34 (2012) 263.
[24] J. De Laat, H. Gallard, *Environmental science & technology,* 33 (1999) 2726-2732.
[25] S.-S. Lin, M.D. Gurol, *Environmental science & technology*, 32 (1998) 1417-1423.
[26] P.M. Gómez-Largo, C.D. Miranda, A.C. Villagrán-Olivares, C.A. López, B.P. Barbero, *Molecular Catalysis*, 530 (2022) 112639.
[27] M.L. Rojas-Cervantes, E. Castillejos, *Catalysts*, 9 (2019) 230.
[28] S. Skounas, C. Methenitis, G. Pneumatikakis, M. Morcellet, *Bioinorganic chemistry and applications*, 2010 (2010) 643120.
[29] A. Hiroki, J.A. LaVerne, *The Journal of Physical Chemistry B*, 109 (2005) 3364-3370.
[30] A. Aguinaco, J.P. Pocostales, J.F. García-Araya, F.J. Beltrán, *Journal of Chemical Technology & Biotechnology*, 86 (2011) 595-600.
[31] L.Trotochaud, S.W.Boettcher,*Scripta Materialia*,74 (2014) 25-32.
[32] X. Xu, F. Song, X. Hu, *Nature Communications*, 7 (2016) 12324.
[33] J.S. Kim, B. Kim, H. Kim, K. Kang, *Advanced Energy Materials*, 8 (2018) 1702774.
[34] S.R. Ede, Z. Luo, *Journal of Materials Chemistry A*, 9 (2021) 20131-20163.
[35] J. Dereń, J. Haber, A. Podgórecka, J. Burzyk, *Journal of Catalysis,* 2 (1963) 161-175.
[36] C.M. Lousada, M. Yang, K. Nilsson, M. Jonsson, *Journal of Molecular Catalysis A: Chemical*, 379 (2013) 178-184.
[37] H. Qiao, Z. Wei, H. Yang, L. Zhu, X. Yan, *Journal of Nanomaterials*, 2009 (2009) 795928.
[38] D. Saravanakkumar, R. Karthika, S. Ganasaravanan, S. Sivaranjani, S. Pandiarajan, B. Ravikumar, A. Ayeshamariam, *J. Appl. Phys*, 10 (2018) 73-83.
[39] M.M. Hussain, M.M. Rahman, A.M. Asiri, *Journal of Environmental Sciences*, 53 (2017) 27-38.
[40] M. El-Kemary, N. Nagy, I. El-Mehasseb, *Materials Science in Semiconductor Processing*, 16 (2013) 1747-1752.
[41] N. Tigau, *Romanian Journal of Physics*, 51 (2006) 641.
[42] H.A. Al-Abadleh, A.B. Voges, P.A. Bertin, Nguyen, F.M. Geiger, *Journal of the American Chemical Society*, 126 (2004) 11126-11127.
[43] M.-K. Tsai, K. Kowalski, M. Valiev, M. Dupuis, *The Journal of Physical Chemistry A*, 111 (2007) 10478-10482.